Phase stability and elastic properties of $Ta_{n+1}AlC_n$ (n = 1–3) at high pressure and elevated temperature

2007 J. Phys.: Condens. Matter 19 136207

(http://iopscience.iop.org/0953-8984/19/13/136207)

IOP PUBLISHING JOURNAL OF PHYSICS: CONDENSED MATTER

J. Phys.: Condens. Matter **19** (2007) 136207 (9pp) doi:10.1088/0953-8984/19/13/136207

Phase stability and elastic properties of $Ta_{n+1}AlC_n$ ($n = 1$–3) at high pressure and elevated temperature

Denis Music[1], **Jens Emmerlich and Jochen M Schneider**

Materials Chemistry, RWTH Aachen University, Kopernikusstraße 16, D-52074 Aachen, Germany

E-mail: music@mch.rwth-aachen.de

Received 22 January 2007, in final form 21 February 2007
Published 13 March 2007
Online at stacks.iop.org/JPhysCM/19/136207

Abstract

We have studied the electronic structure of $Ta_{n+1}AlC_n$ (space group $P6_3/mmc, n = 1$–3) under uniform compression from 0 to 60 GPa and at temperatures from 0 to 1500 K using *ab initio* calculations. These phases can be characterized by alternating layers of high and low electron density and are referred to as nanolaminates. At 0 K we observe similar compressibilities in both the a and c directions for all phases investigated. This is unusual for nanolaminates. Based on the density of states analysis, we propose that these similar compressibilities may be caused by an increase in Ta–Al and Ta–Ta bonding strength as well as a stronger long-range interaction between TaC–TaC layers. No evidence of a phase transition is observed as the pressure is increased to 60 GPa. However, as the temperature is increased to approximately 1000 K without applying pressure, a first-order phase transition occurs in Ta_3AlC_2. These results are relevant for applications of $Ta_{n+1}AlC_n$ at elevated temperature and pressure.

(Some figures in this article are in colour only in the electronic version)

1. Introduction

$Ta_{n+1}AlC_n$ (space group $P6_3/mmc, n = 1$–3) belongs to the so-called MAX phases. These ternary phases can be referred to as nanolaminates and are characterized by alternating MX (M = transition metal, X = C or N) and A layers (mostly IIIA and IVA elements). In general, these ternary phases are good thermal and electrical conductors, are resistant to oxidation and exhibit extensive plasticity [1, 2]. Ta_2AlC ($n = 1$) has been known in the bulk form for more than four decades [3], while Ta_4AlC_3 ($n = 3$) has recently been synthesized in a diamond anvil cell [4] and by hot pressing [5]. Ta_2AlC [6] and Ta_4AlC_3 [4] possess bulk moduli of 251 and 261 GPa, respectively, which are the largest values ever measured for MAX phases. To the best

[1] Author to whom any correspondence should be addressed.

of our knowledge, other physical properties are unknown. The existence of Ta_3AlC_2 ($n = 2$) has not been reported.

Due to the nanolaminated nature of MAX phases and the anisotropy in the chemical bonding [1, 2, 7], it is reasonable to assume that the compressibility of MAX phases is anisotropic. The compressibilities of Ti_2AlC [6], V_2AlC [6], Zr_2InC [8], Ti_3SiC_2 [9], $Ti_3Si_{0.5}Ge_{0.5}C_2$ [10] and Ti_4AlN_3 [11] were measured to be larger along the c than along the a axes, while the opposite was reported for Cr_2AlC [6], Nb_2AlC [6] and Nb_2AsC [12]. The compressibilities of Ta_2AlC [6] were reported to be identical in both directions, whereas the compressibilities of Ta_4AlC_3 [4] are slightly larger in the c direction. Manoun *et al* have suggested that Ta–C bonds are of similar strength to Ta–Al bonds in Ta_4AlC_3 [4], which would explain the compressibility behaviour observed. However, this notion appears to be inconsistent with the measured bulk modulus of Ta_4AlC_3 being only 75.7% of TaC [4]. Also, several reports indicate that MAX phases generally exhibit M–X bonds which are stronger than M–A bonds [1, 2, 7, 13–16].

To the best of our knowledge, the high-temperature behaviour of $Ta_{n+1}AlC_n$ has not been explored. However, other MAX phases of the same stoichiometry have been studied extensively. For instance, Ti_3SiC_2 is known to exhibit two polymorphs, namely α and β [17, 18]. The difference between α-Ti_3SiC_2 and β-Ti_3SiC_2 is that Si atoms occupy the 2b Wyckoff position with the fractional coordinates $(0, 0, 1/4)$ in α-Ti_3SiC_2, while in the β-phase the Si atoms fill the 2d Wyckoff position with the fractional coordinates $(2/3, 1/3, 1/4)$. According to Barsoum [1] and Sun *et al* [19], Ti_3SiC_2 exhibits unusual mechanical properties at elevated temperatures. In contrast to a decrease of flow-stress commonly observed at elevated temperatures, Ti_3SiC_2 demonstrates an increase. In our previous work, we have suggested that the flow stress anomaly in Ti_3SiC_2 can be understood on the basis of a first-order phase transition from α-Ti_3SiC_2 to β-Ti_3SiC_2 at about 1000 K [20]. This is consistent with the experimental data previously reported [19] since Ti_3SiC_2 exhibits a peak flow stress at around 1173 K.

In this work we study the electronic structure of $Ta_{n+1}AlC_n$ ($n = 1$–3) in the pressure range 0–60 GPa and temperature range 0–1500 K using *ab initio* calculations. At 0 K we obtain similar compressibilities in both a and c directions. Based on the density of states analysis, we propose that these similar compressibilities may be caused by an increase in Ta–Al and Ta–Ta bonding strength as well as a stronger long-range interaction between TaC–TaC layers. We also present evidence for a first-order phase transition in Ta_3AlC_2 at approximately 1000 K.

2. Theoretical methods

The *ab initio* approach was used for calculations in this work, which is implemented in the Vienna *ab initio* simulation package (VASP) [21, 22]. Projector augmented wave potentials and the generalized gradient approximation were employed [23], with the so-called Blöchl corrections for the total energy [24]. The integration in the Brillouin zone is done on a special $7 \times 7 \times 7$ k-point mesh determined according to the Monkhorst–Pack method [25]. The convergence criterion for the total energy was 0.01 meV within a 500 eV cut-off. Unit cells containing 8, 12 and 16 atoms for Ta_2AlC, Ta_3AlC_2 (both α and β polymorphs) and Ta_4AlC_3, respectively, were relaxed with respect to atomic positions (internal free parameters), lattice parameter a, i.e. Wigner–Seitz primitive cell volume, and hexagonal c/a ratio. Spin polarisation was not considered [26–28]. The bulk modulus was obtained by fitting the energy–volume curves to the Birch–Murnaghan equation of states [29]. The total and partial density of states (DOS) was calculated.

High-pressure induced changes in the DOS were studied under uniform compression of the equilibrium volume in the pressure range of 0–60 GPa, which is comparable to the previously

Table 1. Lattice parameter (a), hexagonal c/a ratio, equilibrium volume (V_0), bulk modulus (B) and energy of formation (ΔE) for $Ta_{n+1}AlC_n$ ($n = 1$–3), as obtained using the VASP code. In α-Ta_3AlC_2 and β-Ta_3AlC_2 Al atoms occupy the 2b and 2d Wyckoff positions, respectively.

	a (Å)	c/a	V_0 (Å^3/atom)	B (GPa)	ΔE (eV/atom)
Ta_2AlC	3.085[a]	4.549[a]	14.453[a]	222[a]	−0.516
α-Ta_3AlC_2	3.113	6.149	13.391	250	−0.559
β-Ta_3AlC_2	3.096	6.281	13.446	248	−0.543
Ta_4AlC_3	3.146	7.708	12.958	264	−0.569

[a] See reference [36].

studied experimental range [4, 6]. High-temperature induced changes in the electronic structure were studied using the PHONON code [30]. The Helmholtz free energy (F) was obtained from contributions from the lattice vibrations (F_{ph}) and the energy of formation (ΔE) [31]:

$$F = F_{ph} + \Delta E, \tag{1}$$

where ΔE is given as:

$$\Delta E = \frac{E(Ta_{n+1}AlC_n) - 2(n+1)E(Ta) - 2E(Al) - \frac{n}{2}E(C)}{4(n+1)}. \tag{2}$$

E stands for the total energy obtained from the VASP code for unit cells of $Ta_{n+1}AlC_n$ ($n = 1$–3), Ta (space group $Im\bar{3}m$, prototype W, 1 atom/unit cell), Al (space group $Fm\bar{3}m$, prototype Cu, 1 atom/unit cell) and graphite (space group $P6_3/mmc$, prototype graphite, 4 atoms/unit cell), respectively. To determine the lattice dynamics as a function of wavevectors in reciprocal space, the *ab initio* force-constant approach was used, which was implemented by Parlinski *et al* [30]. The summation was constrained to the same reciprocal mesh as for the electronic states. For the phonon calculations, non-equivalent atomic positions were used to generate $2 \times 2 \times 1$ supercells, containing 32, 48 and 64 atoms for Ta_2AlC, Ta_3AlC_2 (both α and β polymorphs) and Ta_4AlC_3, respectively. In order to avoid interaction between the two images of a displaced atom (due to the periodical boundary condition), it is necessary to use a relatively large supercell for the calculations of the force matrices. Each supercell was subjected to 9–15 non-equivalent deformations with 3% displacements. Hellmann–Feynman forces, obtained from the force-constant matrices, were evaluated. The dynamical matrices are solved by a direct method based on the harmonic approximation [30].

3. Results and discussion

We start the analysis of the *ab initio* results obtained by comparing the equilibrium volume and the bulk modulus to previously reported experimental data [4, 6]. Table 1 contains calculated lattice parameters, equilibrium volume, bulk modulus and energy of formation of $Ta_{n+1}AlC_n$ ($n = 1$–3). The calculated equilibrium volume of Ta_2AlC and Ta_4AlC_3 deviates from the experimental values [6, 4] by 1.1% and 5.8%, respectively. Previously we have investigated the influence of N vacancies on structure, relative phase stability, as well as elastic and transport properties of Ti_4AlN_3, an isostructural compound to Ta_4AlC_3, and determined that a N vacancy population of 3.2% can be accommodated by decreasing the equilibrium volume by 0.7%, without significant reduction of the bulk modulus [32]. It may be speculated that if C vacancies are formed in Ta_4AlC_3, similar behaviour may be observed. This hypothesis may be tested by transmission electron microscopy or structural refinements from diffraction data. The calculated bulk modulus of Ta_2AlC and Ta_4AlC_3 deviates by 11.6% and 1.1%, respectively, from the experimental values [6, 4]. The energy of formation with respect to the

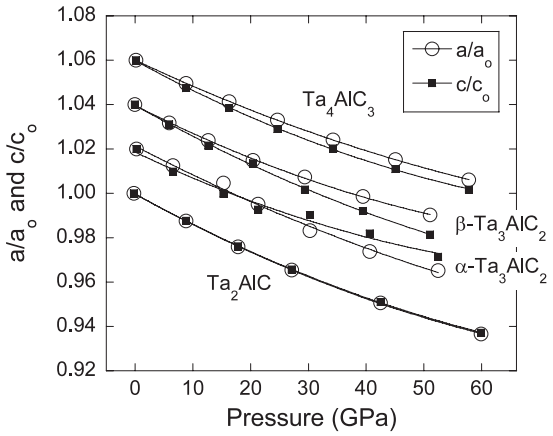

Figure 1. Lattice parameters (a and c) relative to the zero-pressure values (a_0 and c_0) for $Ta_{n+1}AlC_n$ ($n = 1$–3) at 0 K. Second-order polynomials are used to fit the data. For the convenience of the reader, curves are shifted by 0.02 from one another.

Table 2. Relative changes in lattice parameter for $Ta_{n+1}AlC_n$ ($n = 1$–3) as a function of pressure (P) given in GPa. Two polymorphs are given for $n = 2$.

$Ta_{n+1}AlC_n$	a/a_0	c/c_0
$n = 1$	$1 - 0.0014P + 6.4 \times 10^{-6}P^2$	$1 - 0.0014P + 6.3 \times 10^{-6}P^2$
$n = 2(\alpha)$	$1 - 0.0014P + 5.0 \times 10^{-6}P^2$	$1 - 0.0012P + 7.0 \times 10^{-6}P^2$
$n = 2(\beta)$	$1 - 0.0013P + 7.2 \times 10^{-6}P^2$	$1 - 0.0015P + 6.2 \times 10^{-6}P^2$
$n = 3$	$1 - 0.0012P + 5.0 \times 10^{-6}P^2$	$1 - 0.0014P + 7.1 \times 10^{-6}P^2$

elements decreases from −0.516 to −0.569 eV/atom as n increases from 1 to 3 (see table 1). Moreover, α-Ta_3AlC_2 is 16 meV/atom more stable than β-Ta_3AlC_2, which is consistent with the theoretical stability behaviour of the Ti_3SiC_2 polymorphs, where a 0.01 eV/atom energy difference results in a phase transition at about 1000 °C [20].

In figure 1, relative changes in the lattice parameters are plotted as a function of pressure during uniform compression at a temperature of 0 K. Least square fits of these curves are given in table 2. The compressibilities in a and c directions are identical for Ta_2AlC, whereas Ta_4AlC_3 is slightly more compressible along the c axes. The high-pressure behaviour of Ta_2AlC and Ta_4AlC_3 calculated here is thus in good agreement with previously reported experimental data [4, 6]. Based on the compressibility data for Ta_4AlC_3, Manoun *et al* have suggested that Ta–C bonds are of similar strength to Ta–Al bonds [4]. In order to test this bonding-strength hypothesis, we studied the bond stiffness in $Ta_{n+1}AlC_n$ ($n = 1$–3), which is given in figure 2. The bond stiffness was obtained by fitting the relative bond length as a function of pressure with second-order polynomials. It is evident that Ta–C bonds are stiffer than Ta–Al bonds. This is consistent with the literature claiming that M–X bonds are stronger than M–A bonds [1, 2, 7, 13–16]. This also explains the larger bulk modulus value TaC (345 GPa) compared to Ta_4AlC_3 (261 GPa) [4]. This is expected due to the bond strength anisotropy in the ternary phase. Furthermore, the high-pressure behaviour of the hypothetical Ta_3AlC_2 polymorphs is similar to Ti_3SiC_2 [33, 34].

In order to identify the origin of the rather unusual compressibility behaviour of $Ta_{n+1}AlC_n$ ($n = 1$–3), we analyse the DOS at a pressure of 0 GPa (figure 3) and at 60 GPa, which was the maximum pressure investigated (figure 4). The DOS analysis was carried out at a temperature

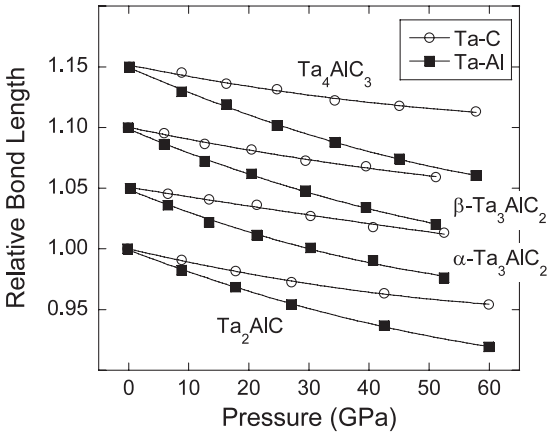

Figure 2. Ta–C and Ta–Al bond length relative to the zero-pressure values for $Ta_{n+1}AlC_n$ ($n = 1$–3) at 0 K. Second-order polynomials are used to fit the data. For the convenience of the reader, curves are shifted by 0.05 from one another.

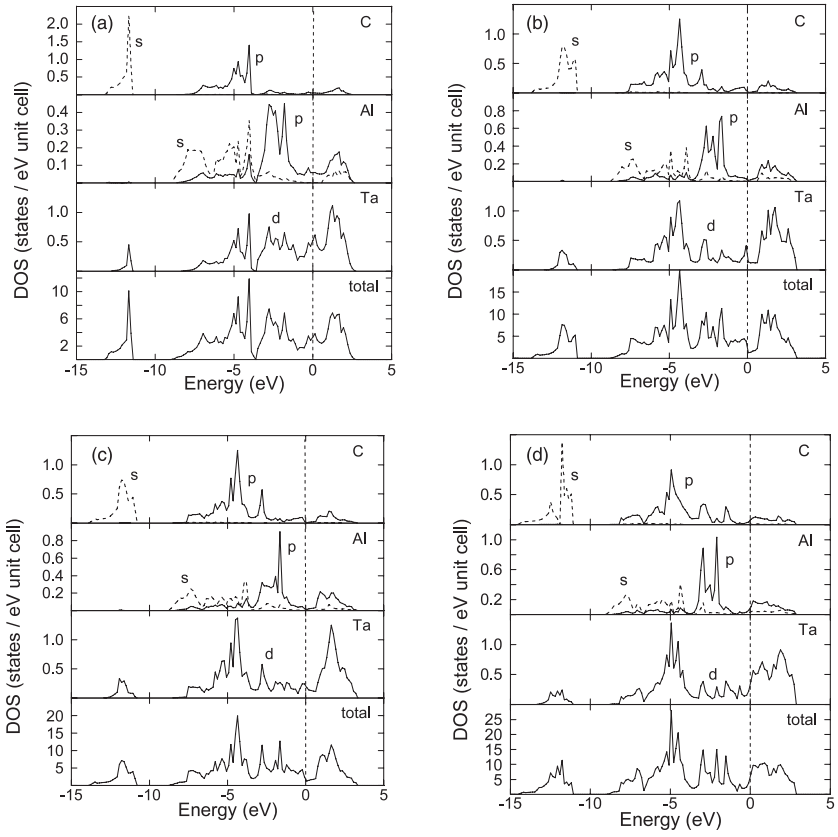

Figure 3. Partial and total DOS for (a) Ta_2AlC, (b) α-Ta_3AlC_2, (c) β-Ta_3AlC_2 and (d) Ta_4AlC_3 at a pressure of 0 GPa and 0 K. The Fermi level is set to 0 eV and indicated by a vertical dashed line.

of 0 K. The total and partial DOS data for Ta_2AlC (figure 3(a)), α-Ta_3AlC_2 (figure 3(b)), β-Ta_3AlC_2 (figure 3(c)) and Ta_4AlC_3 (figure 3(d)) are rather similar. The Ta 5d and C 2p states

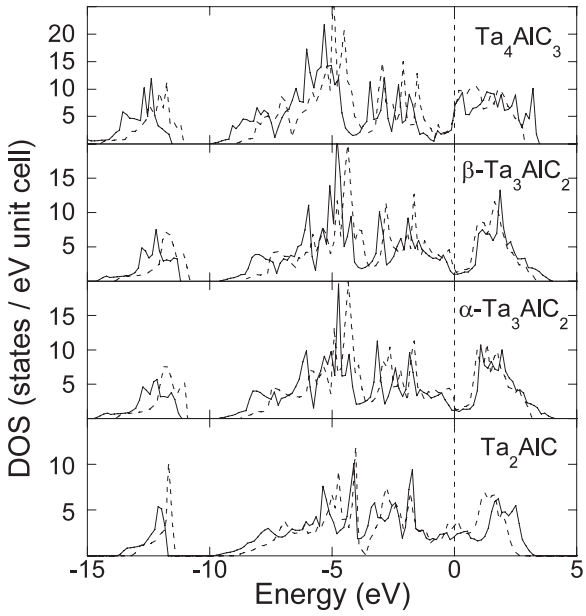

Figure 4. Comparison of total DOS for $Ta_{n+1}AlC_n$ ($n = 1$–3) at 0 K and pressures of 0 GPa (dashed line) as well as the highest pressure applied (solid line). The Fermi level is set to 0 eV and indicated by a vertical dashed line.

are hybridized in the range from approximately −8 to −4 eV. Ta 5d and Al 3p orbitals are hybridized in the range from approximately −8 up to the Fermi level, indicating that the Ta–C bonds are stronger than Ta–Al bonds. This is consistent with our bond stiffness data discussed above. When states of different symmetry form hybrids, such as M d–A p, the DOS may in turn be split into bonding and antibonding (or non-bonding) contributions [35]. Thus, the Ta 5d and Al 3p hybridization exhibits a pseudogap at about −3.7 eV, but since it is not close to the Fermi level, antibonding contributions are not expected. The Fermi level is mainly occupied by Ta 5d states, giving rise to relatively weak metallic Ta–Ta bonding and in general a metallic character of these compounds. These results are consistent with the previously published data on the chemical bonding in MAX phases [7, 13–16, 36, 37].

As $Ta_{n+1}AlC_n$ ($n = 1$–3) compounds are subjected to the maximum pressure applied (see figure 4), the most significant change is the shift of all states to lower energies. This implies that the population of Ta 5d increases, the pseudogap in the Ta–Al hybridization shifts below −3.7 eV and the Ta–C bonds become stronger. The shift of the pseudogap in the Ta–Al hybridization suggests Ta–Al bond strengthening under compression [7, 37]. No evidence for a change in the nature of the bonding is observed, indicating that the phases studied may be stable in the pressure range probed. The increase in the population of Ta 5d states may cause three effects: (1) stronger Ta–C bonds, as already pointed out, (2) stronger long-range interaction between TaC–TaC layers and (3) stronger Ta–Ta bonds. These three effects may contribute towards a decrease in compressibilities in both a and c directions. The long-range interaction between MC–MC layers was considered in our previous work where the electronic origin of shearing in M_2AlC phases was studied [38–40]. Based on the decomposed band structure analysis, it was observed that the MC–MC interaction contributes to shearing. This is also consistent with the stress–strain analysis [38, 41], based on the deformation induced through C_{44} elastic constant [42] and basal slip. It is reasonable to assume that the stronger long-

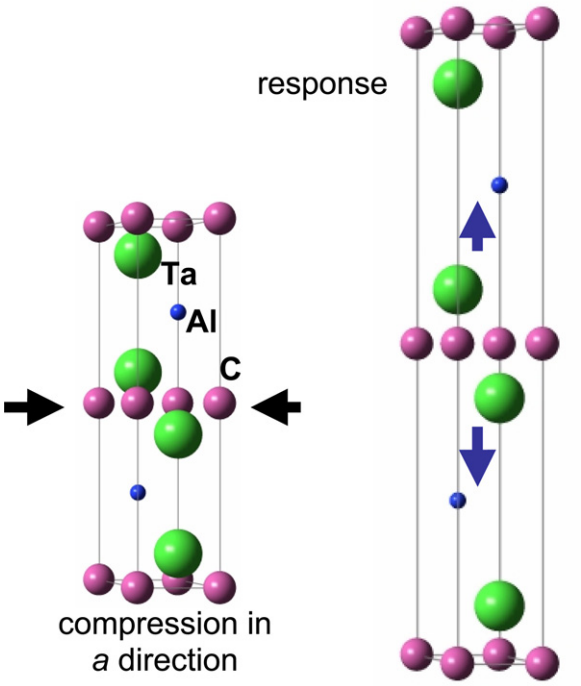

Figure 5. Deformation of Ta_2AlC under uniform compression.

range interaction between TaC–TaC layers may also contribute to a decrease in compressibility in the c direction. The third effect, i.e. stronger Ta–Ta bonds, may also be relevant for the compressibility. We have previously performed studies of the solubility within $Nb_{2-x}W_xAlC$ by means of *ab initio* calculations and found that both the Nb–C bond length as well as the W–C bond length are not significantly affected by variations in x [43]. This can be understood by studying the C–M–M angle. An increase in the $CNb_{2-x}W_x$ bond angle is consistent with the notion of flattening $Nb_{2-x}W_xC$ layers [43]. This is enabled by relatively weak and hence easily deformable M–M bonds within the carbidic layer. Uniform compression can be described as a simultaneous in-plane compression and a compression in the c direction. Figure 5 is a schematic drawing illustrating the response of Ta_2AlC to uniform compression based on our DOS analysis. Under in-plane compression, stiff Ta–C building blocks rearrange due to the presence of metallic Ta–Ta bonds, which thus may oppose the compression in the c direction. This in turn provides a decreased compressibility in the c direction and is consistent with the notion of Ta–Ta bond strengthening under uniform compression. Therefore, we propose that the cause of the similar compressibilities in a and c directions of $Ta_{n+1}AlC_n$ ($n = 1$–3) may be an increase in Ta–Al and Ta–Ta bond strength as well as the stronger long-range interaction between TaC–TaC layers.

Figure 6 shows the Helmholtz free energy for $Ta_{n+1}AlC_n$ ($n = 1$–3), which is, according to equation (1), a sum of the energy of formation with respect to elements (given in table 1) and harmonic phonon free energy calculated using the total phonon DOS. The Helmholtz free energy was obtained at a pressure of 0 GPa. All phases studied are stable in the temperature range probed. Identical Helmholtz free energy values for α-Ta_3AlC_2 and β-Ta_3AlC_2 are obtained at a temperature of approximately 1000 K. The phase transition observed is of the first

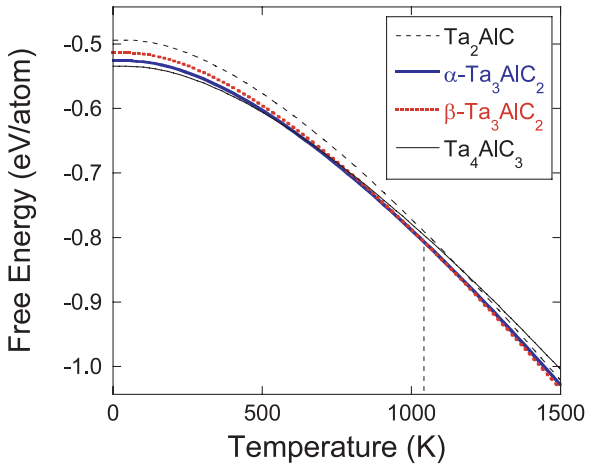

Figure 6. Free energy for $Ta_{n+1}AlC_n$ ($n = 1$–3) at a pressure of 0 GPa. The vertical dashed line indicates the transition temperature for Ta_3AlC_2.

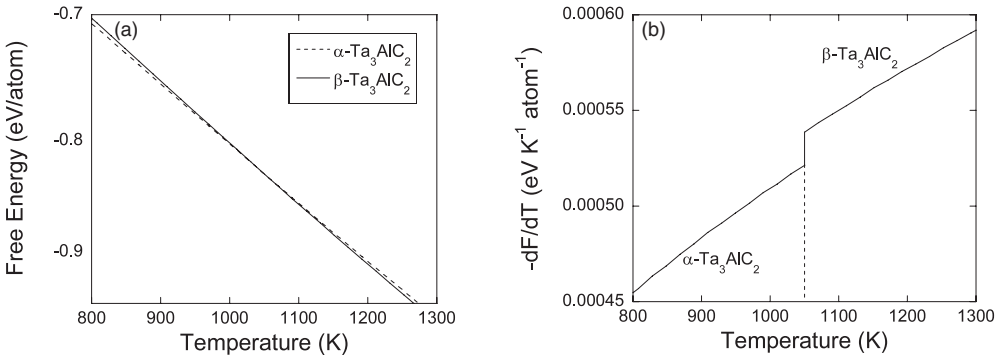

Figure 7. (a) Free energy (F) for Ta_3AlC_2 as a function of temperature (T) at a pressure of 0 GPa. (b) dF/dT for Ta_3AlC_2 showing the transition temperature indicated by a vertical dashed line.

order, Al atoms move from the 2b to the 2d Wyckoff position. In order to show the change in the slope of the Helmholtz free energy for Ta_3AlC_2, the Helmholtz free energy and its derivative with respect to temperature in the transition temperature region are given in figure 7. This phase transition is consistent with the behaviour of Ti_3SiC_2 [17, 18, 20]. Hence, $Ta_{n+1}AlC_n$ ($n = 1$–3) compounds may be suitable for high-temperature and high-pressure applications.

4. Conclusions

We have studied the electronic structure of $Ta_{n+1}AlC_n$ under uniform compression in the range of 0–60 GPa and at elevated temperatures in the range of 0–1500 K using *ab initio* calculations. At 0 K, we observe similar compressibilities in both a and c directions. This is unusual for nanolaminates. This behaviour can be understood based on the density of states analysis. We suggest that the similar compressibilities of $Ta_{n+1}AlC_n$ ($n = 1$–3) in the a and c directions are facilitated by an increase in Ta–Al and Ta–Ta bonding strength as well as a stronger long-range interaction between TaC–TaC layers due to the shift of all states to lower energies. No evidence of a phase transition is observed as the pressure is increased to 60 GPa. However, as the temperature is increased to approximately 1000 K without applying pressure, a first-order phase

transition occurs in Ta_3AlC_2. It is our ambition that these results will spark more experimental interest and enable applications of $Ta_{n+1}AlC_n$ at elevated temperature and pressure.

Acknowledgment

We acknowledge support from DFG (Schn 735/8-1, 'Mechanical properties of MAX phase thin films').

References

[1] Barsoum M W 2000 *Prog. Solid State Chem.* **28** 201
[2] Barsoum M W and El-Raghy T 2001 *Am. Sci.* **89** 334
[3] Jeitschko W, Nowotny H and Benesovsky F 1963 *Monatsch. Chem.* **94** 672
[4] Manoun B, Saxena S K, El-Raghy T and Barsoum M W 2006 *Appl. Phys. Lett.* **88** 201902
[5] Lin Z J, Zhuo M J, Zhou Y C, Li M S and Wang J Y 2006 *J. Mater. Res.* **21** 2587
[6] Manoun B, Gulve R P, Saxena S K, Gupta S, Barsoum M W and Zha C S 2006 *Phys. Rev.* B **73** 024110
[7] Music D, Sun Z, Ahuja R and Schneider J M 2006 *Phys. Rev.* B **73** 134117
[8] Manoun B, Saxena S K, Liermann H P, Gulve R P, Hoffman E, Barsoum M W, Hug G and Zha C S 2004 *Appl. Phys. Lett.* **85** 1514
[9] Jordan J L, Sekine T, Kobayashi T, Li X, Thadhani N N, El-Raghy T and Barsoum M W 2003 *J. Appl. Phys.* **93** 9639
[10] Manoun B, Liermann H P, Gulve R P, Saxena S K, Ganguly A, Barsoum M W and Zha C S 2004 *Appl. Phys. Lett.* **84** 2799
[11] Manoun B, Saxena S K and Barsoum M W 2005 *Appl. Phys. Lett.* **86** 101906
[12] Kumar R S, Rekhi S, Cornelius A L and Barsoum M W 2005 *Appl. Phys. Lett.* **86** 111904
[13] Sun Z, Ahuja R, Li S and Schneider J M 2003 *Appl. Phys. Lett.* **83** 899
[14] Wang J and Zhou Y 2004 *Phys. Rev.* B **69** 214111
[15] Hug G, Jaouen M and Barsoum M W 2005 *Phys. Rev.* B **71** 024105
[16] Grechnev A, Li S, Ahuja R, Eriksson O, Jansson U and Wilhelmsson O 2004 *Appl. Phys. Lett.* **85** 3071
[17] Farber L, Levin I, Barsoum M W, El-Raghy T and Tzenov T 1999 *J. Appl. Phys.* **86** 2540
[18] Yu R, Zhan Q, He L L, Zhou Y C and Ye H Q 2002 *J. Mater. Res.* **17** 948
[19] Sun Z, Zhou Y and Zhou J 2000 *Phil. Mag. Lett.* **80** 289
[20] Sun Z, Zhou J, Music D, Ahuja R and Schneider J M 2006 *Scr. Mater.* **54** 105
[21] Kresse G and Hafner J 1993 *Phys. Rev.* B **48** 13115
[22] Kresse G and Hafner J 1994 *Phys. Rev.* B **49** 14251
[23] Kresse G and Joubert D 1999 *Phys. Rev.* B **59** 1758
[24] Blöchl P E 1994 *Phys. Rev.* B **50** 17953
[25] Monkhorst H J and Pack J D 1976 *Phys. Rev.* B **13** 5188
[26] Schneider J M, Sun Z, Mertens R, Uestel F and Ahuja R 2004 *Solid State Commun.* **130** 445
[27] Music D, Sun Z, Ahuja R and Schneider J M 2006 *J. Phys.: Condens. Matter* **18** 8877
[28] Schneider J M, Mertens R and Music D 2006 *J. Appl. Phys.* **99** 013501
[29] Birch F 1978 *J. Geophys. Res.* **83** 1257
[30] Parlinski K, Li Z Q and Kawazoe Y 1997 *Phys. Rev. Lett.* **78** 4063
[31] Parlinski K and Parlinska-Wojtan M 2002 *Phys. Rev.* B **66** 064307
[32] Music D, Ahuja R and Schneider J M 2005 *Appl. Phys. Lett.* **86** 031911
[33] Onodera A, Hirano H, Yuasa T, Gao N F and Miyamoto Y 1999 *Appl. Phys. Lett.* **74** 3782
[34] Fang C M, Ahuja R, Eriksson O, Li S, Jansson U, Wilhelmsson O and Hultman L 2006 *Phys. Rev.* B **74** 054106
[35] Gelatt C D Jr, Williams A R and Moruzzi V L 1983 *Phys. Rev.* B **27** 2005
[36] Schneider J M, Music D and Sun Z 2005 *J. Appl. Phys.* **97** 066105
[37] Sun Z, Music D, Ahuja R, Li S and Schneider J M 2004 *Phys. Rev.* B **70** 092102
[38] Music D, Sun Z, Voevodin A A and Schneider J M 2006 *Solid State Commun.* **139** 139
[39] Music D, Sun Z, Voevodin A A and Schneider J M 2006 *J. Phys.: Condens. Matter* **18** 4389
[40] Sun Z, Music D, Ahuja R and Schneider J M 2005 *J. Phys.: Condens. Matter* **17** 7169
[41] Liao T, Wang J and Zhou Y 2006 *Phys. Rev.* B **73** 214109
[42] Fast L, Wills J M, Johansson B and Eriksson O 1995 *Phys. Rev.* B **51** 17431
[43] Schneider J M, Sun Z and Music D 2005 *J. Phys.: Condens. Matter* **17** 6047